Agenzia Spaziale Italiana

Astronaut Radiation Dose Calculation With a New Galactic Cosmic Ray Model and the AMS-02 Data

Xuemei C. et. al.

Research Article:
17 April 2023
10.1029/2022SW003285

I gratefully acknowledge the strong support from the AMS collaboration and from the Italian Space Agency (ASI) within the agreement ASI-INFN n. 2019-19-HH.0.

Abstract We present a new calculation of the astronaut dose rate from the galactic cosmic rays in free space at 1 AU. We use the unshielded isotropic fluence-to-dose conversion coefficients given in the International Commission on Radiological Protection publication 123. A new 3D and time-dependent solar modulation model based on Parker's transport equation as originally developed by Song et al. (2021, https:// doi.org/10.3847/1538-4365/ac281c) is used to calculate the galactic cosmic ray spectra at 1 AU. This model uses the recent local interstellar spectra of Corti et al. (2019, https://doi.org/10.3847/1538-4357/aafac4), M. J. Boschini et al. (2020, https://doi.org/10.3847/1538-4365/aba901, 2021a, https://doi.org/10.3847/1538-4357/ abf11c) to reproduce the PAMELA and AMS-02 observations between 2006 and 2019. The radiation dose calculated from our model and from the AMS-02 spectra in the same rigidity region agrees better than 1% for proton and helium in a time-dependent way, and at 2% level for the six most contributing cosmic ray elements averaged over 7 or 8.5 years. The time-dependent dose rate analysis over 13 years shows an effective dose equivalent rate of 55–58 cSv/yr at solar minimum (January 2010) and 26 cSv/yr at solar maximum (February 2014).

Outline of the presentation

The Sketch Summary of the Paper

Q(R,E) $ICRP_{60}$

Q(R,E) NASA

Tissue weighting factor (WT)

Equivalent Dose rate ($H_{T,R}$) $\sum_T w_T H_{T,R}$ Effective Dose Equivalent rate ($H_{E,R}$) $\sum_R H_{E,R}$ Total Effective Dose Equivalent rate (H_E)

AMS data

Local Interstellar Spectra (LIS)

3D &T.M. (GCR model)

N.E.S.

SPECT(R)
17 /07/ 2006 to 31 /10/ 2019
Bartel Rotation 2360 - 2540

The time series for effective dose equivalent rates and skin dose equivalent rates in the time window (17 July 2006 to 31 October 2019), with genders averaged but two quality factors shown.

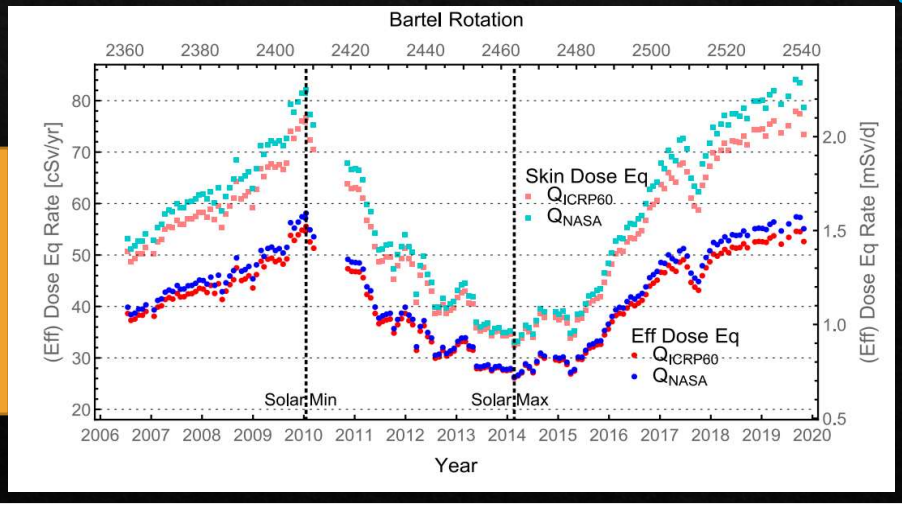

1. Introduction (1/2)

AMS-02 experiment on the International Space Station, the galactic cosmic ray (GCR) spectra are measured with unprecedented precision and statistics.

The high charge and energy particles, and the rigidity range of $\gtrsim$1 GV are the most important for astronaut dosimetry.

This paper reported the calculation of various astronaut dose rates due to the GCR, aiming to fully use the precision of the AMS-02 direct measurements.

Therefore, the major goal of the paper is to improve the calculation precision of astronaut radiation dose induced by the energetic cosmic ray from outside the solar system, with the help of the AMS-02 data.

- It presented a new calculation of the astronaut dose rate from the galactic cosmic rays in free space at 1 AU, using the unshielded isotropic fluence-to-dose conversion coefficients given in the International Commission on Radiological Protection publication 123.
- A new 3D and time-dependent solar modulation model based on Parker's transport equation is used for the dose calculation.

1. Introduction (2/2)

- This model uses the recent local interstellar spectra (LIS) to reproduce the PAMELA and AMS-02 observations between 2006 and 2019.

- For the GCR spectra side, since the AMS-02 measurement cannot be used directly as the input, a recent 3D and time-dependent GCR numerical model (GCR model) was used as spectrum generation for the dosimetry calculation, together with the local interstellar spectra as a boundary condition.

- The GCR spectra were integrated with the fluence-to-dose conversion coefficient to obtain the dose equivalent contribution.

The Sketch Summary of the Mathematical part

Q(R,E) $ICRP_{60}$

Q(R,E) NASA

Tissue weighting factor (WT)

Equivalent Dose rate ($H_{T,R}$) $\sum_T w_T H_{T,R}$ Effective Dose Equivalent rate ($H_{E,R}$) $\sum_R H_{E,R}$ Total Effective Dose Equivalent rate (H_E)

AMS data

Local Interstellar Spectra (LIS)

3D &T.M. (GCR model)

N.E.S.

SPECT(R)
17 /07/ 2006 to 31 /10/ 2019
Bartel Rotation 2360 - 2540

The time series for effective dose equivalent rates and skin dose equivalent rates in the time window (17 July 2006 to 31 October 2019), with genders averaged but two quality factors shown.

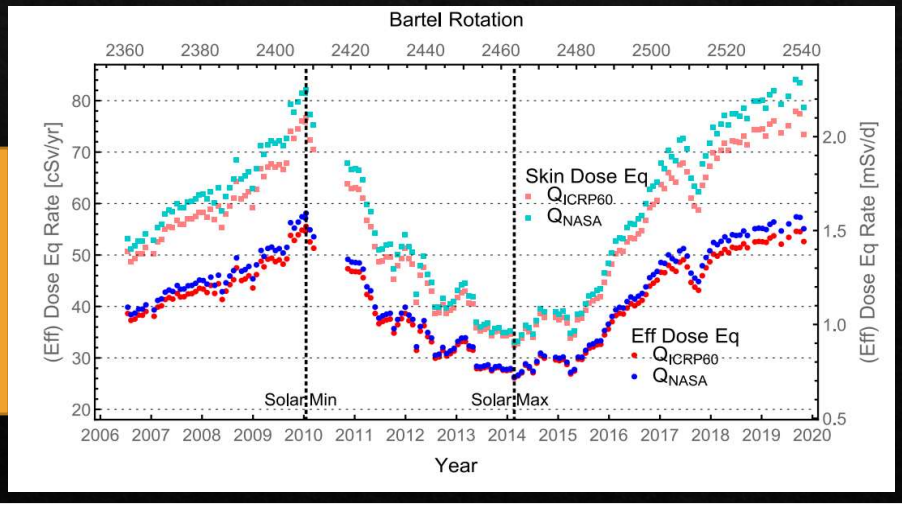

1.1 Mathematical Methodology (1/2)

Equ. 1 indicates, the GCR spectra integrated with the fluence-to-dose coefficient to obtain *the dose-equivalent* contribution:

Where:

- $\boldsymbol{R} = pc/(Ze)$ is the rigidity,
- N_{R} is the number of incident particles of radiation type R
- A is the cross-section of the flux.
- $J_{\mathrm{R}}(\boldsymbol{R})$ is the isotropic flux measured in (m^2 x s x sr x GV)$^{-1}$, and integration with time is also implied to return to $d^2N_{\mathrm{R}}/dAd\boldsymbol{R}$ and obtain dose.
- The absorbed dose $D_{T,\mathrm{R}} = dE_{T,\mathrm{R}}/dm$ is the energy $E_{T,\mathrm{R}}$ deposited per unit mass into tissue/organ "T" induced by such N_{R} particles,
- Φ is the fluence, and
- Q is the quality factor.

$$H_{T,\mathrm{R}} = \int d\boldsymbol{R} \left(\frac{d^2N_{\mathrm{R}}}{dAd\boldsymbol{R}}\right)\left(\frac{D_{T,\mathrm{R}}Q}{dN_{\mathrm{R}}/dA}\right)$$

$$= \int d\boldsymbol{R}\, 4\pi\, J_{\mathrm{R}}(\boldsymbol{R})\, (D_{T,\mathrm{R}}/\Phi)(\boldsymbol{R})\, Q \qquad (1)$$

1.1 Mathematical Methodology (2/2)

A summation over the human sensitive tissue/organ with the tissue weighting factor w_T of dose equivalent:

gives the effective dose equivalent from a specific radiation species, and a summation over the GCR radiation species gives the ***total effective dose equivalent****.*

The fluence-to-dose conversion coefficient ${}^{D_{T,R}\,Q}/_{(dN_R/dA)}$ with dimension Sv x m^2 has the physical meaning of the expected dose equivalent caused by a single particle of certain type and energy/rigidity to certain human tissue/organ, if the incident particle is integrated over all contributing cross section and averaged over directions assuming isotropy.

$$H_{E,\mathrm{R}} = \sum_T w_T H_{T,\mathrm{R}} \qquad (2)$$

$$H_{E,\mathrm{R}} = \sum_T w_T \int d\boldsymbol{R}\, 4\pi\, J_{\mathrm{R}}(\boldsymbol{R})\, (D_{T,\mathrm{R}}/\Phi)(\boldsymbol{R})\, Q$$

... (3)

The Sketch Summary of the GCR Model

Q(R,E) $ICRP_{60}$

Q(R,E) NASA

Tissue weighting factor (WT)

Equivalent Dose rate ($H_{T,R}$) $\sum_T w_T H_{T,R}$ Effective Dose Equivalent rate ($H_{E,R}$) $\sum_R H_{E,R}$ Total Effective Dose Equivalent rate (H_E)

AMS data

Local Interstellar Spectra (LIS)

3D &T.M. (GCR model)

N.E.S.

SPECT(R)
17 /07/ 2006 to 31 /10/ 2019
Bartel Rotation 2360 - 2540

The time series for effective dose equivalent rates and skin dose equivalent rates in the time window (17 July 2006 to 31 October 2019), with genders averaged but two quality factors shown.

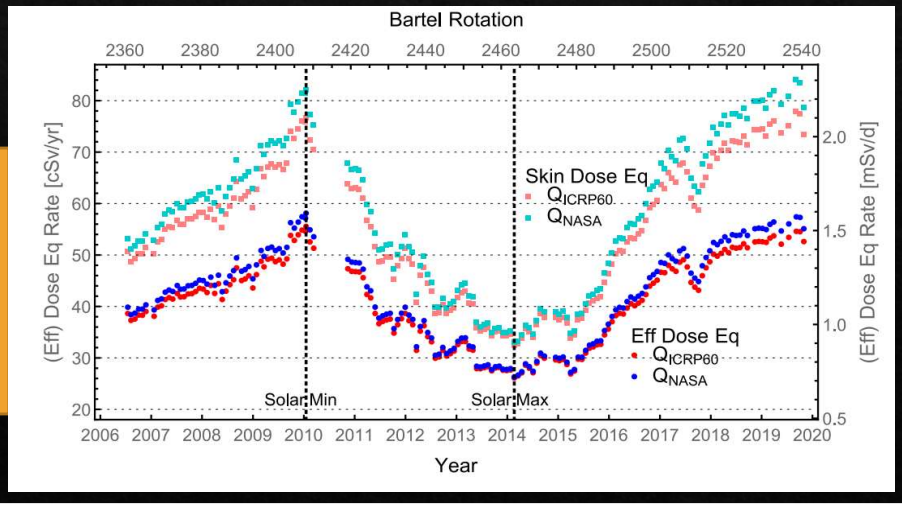

2. The GCR Model (1/2)

On the GCR spectra side:

A recent 3D and time-dependent GCR numerical model were used as the spectrum generator for our dosimetric calculation, together with the local interstellar spectra as boundary conditions.

The original Parker's transport equation for the phase space density $f(\vec{r}, p)$ is given by equ. 4:

In principle $\vec{v}_d$ and $\vec{K}$ are determined by time-dependent observational heliospheric parameters only (e.g., the solar wind speed, the heliospheric current sheet tilt angle, the heliospheric magnetic field strength and its polarity).

$$\frac{\partial f}{\partial t} = (\vec{v}_{sw} + \vec{v}_d) . \nabla f + \frac{1}{3}(\nabla . \vec{v}_{sw}) \frac{\partial f}{\partial \ln p} + \nabla . (\vec{K} . \nabla f) \quad \ldots (4)$$

where $\vec{v}_{sw}$ and $\vec{v}_d$ are the background solar wind and pitch angle averaged drift velocities respectively, and $\vec{K}$ is the diffusion coefficient tensor.

2. The GCR Model (2/2)

In practical calculation, Equation (5) is reformulated into an equivalent stochastic differential equation (SDE) set for the GCR phase space coordinates.

Here s = −t is the backward time.

The differential random noises $d\vec{W}$ superimposed on the deterministic motion describe the Wiener diffusion process, which are given by the small scale heliospheric magnetic field irregularity.

$$d\vec{r} = \left(\nabla . \vec{K} - \vec{V}_{sw} - \vec{v}_d\right)ds + \vec{\sigma} . d\vec{W} \quad with \quad \vec{\sigma} . \vec{\sigma} = 2\vec{K}$$

... (5)

$$dp = \frac{1}{3} p(\nabla . \vec{v}_{sw})ds \qquad (6)$$

2.1 The Extension Beyond the AMS-02 Measured Rigidity Minimum

In Figure 1 it is shown, the AMS-02 measured spectra as well as the calculated spectra for proton and iron.

One important limitation of the AMS-02 results is that at the low rigidity side, the measurement has a finite rigidity minimum, which is mainly due to the energy loss process in the detector and should not be confused with the geomagnetic "cutoff."

The measured spectra have minimums at 1 GV for proton and 2.65 GV for iron respectively.

For such a spectrum, the effective dose equivalent (rate) from a specific radiation species can only be calculated above the minimum "$\boldsymbol{R}_M$" as:

$$H_{E,\mathrm{R}}(\boldsymbol{R}_w) = \sum_T w_T \int_{\boldsymbol{R}_M}^{\infty} d\boldsymbol{R}\, 4\pi\, J_{\mathrm{R}}(\boldsymbol{R}) \left(\frac{D_{T,R}}{\Phi}\right)(\boldsymbol{R}) Q \qquad \ldots (7)$$

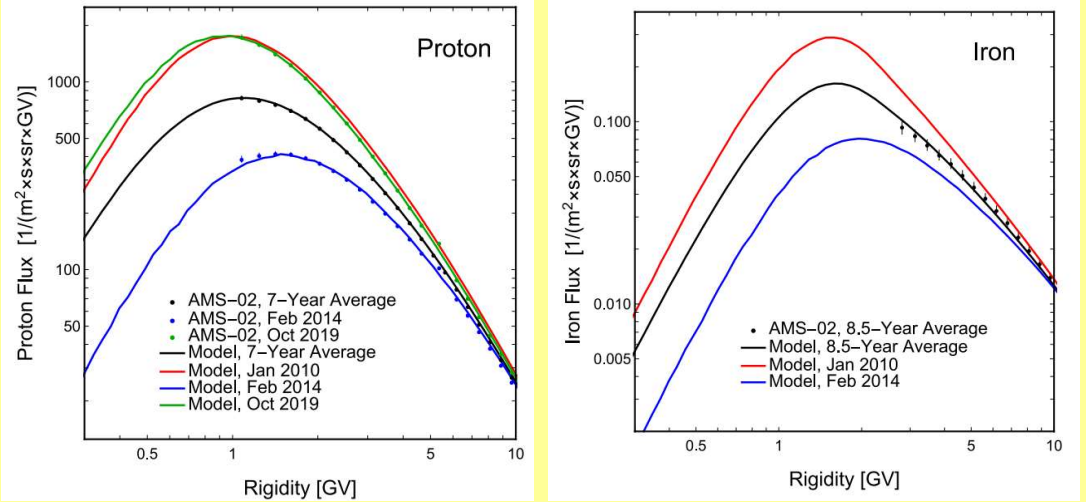

Figure 1. *The comparison between the AMS-02 measured spectra (data points) and the model calculation (curves). In the left (right) panel the measured average flux for proton (iron) during 7 (8.5) years is taken from Aguilar et al., and the calculated average flux is the numerical average of the same 7 (8.5) years flux. From the daily proton flux data, the solar maximum and solar minimum spectra were calculated as the corresponding monthly average. However, the true solar minimum of January 2010 in the time window was not covered, so it was chosen to plot the flux for October 2019 (the last available month) which was the closest to the next solar minimum instead.*

2.2 The Extension to the Elements Absent in AMS-02 Measurements (1/2)

Currently, the AMS-02 has published measurements for the Z = 1–14 and Z = 26 elements. For the elements which have not yet been measured by AMS-02, the GCR model is used to calculate their spectra. Including all the high Z and energy GCR species, all the 28 GCR spectra are calculated at 1 AU point by point in a time series.

Table 1

Comparison of the Averaged $H_{E,R}$ Rate as Numerically Averaging the Rate Time Series Calculated From Model, to the $H_{E,R}$ Rate Directly Calculated Using the Measured AMS-02 7-Year (or 8.5-Year) Averaged Spectra (Aguilar, Cavasonza, Allen, et al., 2021; Aguilar et al., 2020, 2021a)

		p	He	O	Mg	Si	Fe
	Minimum $\mathcal{R}_M$ [GV]	1	1.92	2.15	2.15	2.15	2.65
Q_{ICRP60}	$H_{E,R,Model}(\mathcal{R}_M)$ rate [cSv/yr]	9.26	2.80	0.94	1.09	1.55	3.95
	$H_{E,R,AMS\text{-}02}(\mathcal{R}_M)$ rate [cSv/yr]	9.23	2.84	0.97	1.11	1.52	4.00
	$H_{E,R,Model}(\mathcal{R}_M)/H_{E,R,AMS\text{-}02}(\mathcal{R}_M) - 1$	**0.3%**	**−1.4%**	**−2.3%**	**−2.2%**	**1.9%**	**−1.4%**
	$1 - H_{E,R,Model}(\mathcal{R}_M)/H_{E,R,Model}$	13.6%	30.3%	63.2%	45.3%	37.3%	25.7%
Q_{NASA}	$H_{E,R,Model}(\mathcal{R}_M)$ rate [cSv/yr]	11.61	3.52	0.91	0.79	1.09	3.15
	$H_{E,R,AMS\text{-}02}(\mathcal{R}_M)$ rate [cSv/yr]	11.58	3.57	0.93	0.81	1.07	3.18
	$H_{E,R,Model}(\mathcal{R}_M)/H_{E,R,AMS\text{-}02}(\mathcal{R}_M) - 1$	**0.2%**	**−1.4%**	**−2.3%**	**−2.2%**	**2.0%**	**−0.9%**
	$1 - H_{E,R,Model}(\mathcal{R}_M)/H_{E,R,Model}$	12.4%	28.0%	65.7%	52.7%	44.7%	30.9%

Note. For p, He, O, Mg, and Si, the time window is from May 2011 to May 2018, and for Fe the time window is from May 2011 to October 2019. The measured AMS-02 spectra have minimums at low rigidities, so we make the same cuts on the model side. However still some part of dose are from the GCR below $\mathcal{R}_M$, so the fraction below the cut is also shown. Here the effective dose equivalent rates are averaged over genders. Bold values represent that they are more important than the surrounding values and deserve attention in a first glance.

2.2 The Extension to the Elements Absent in AMS-02 Measurements (2/2)

In Figure 2, it is shown the unshielded gender averaged effective dose equivalent fractional contributions for all the 28 elements, respectively at the solar minimum and maximum, and respectively with the quality factor definition of ICRP60 and NASA.

We can see that the top six contributing elements are always proton (p), helium (He), oxygen (O), magnesium (Mg), silicon (Si), and iron (Fe), and the six elements add more than 74% of the total contribution.

The individual contribution from the other elements is always below 5%.

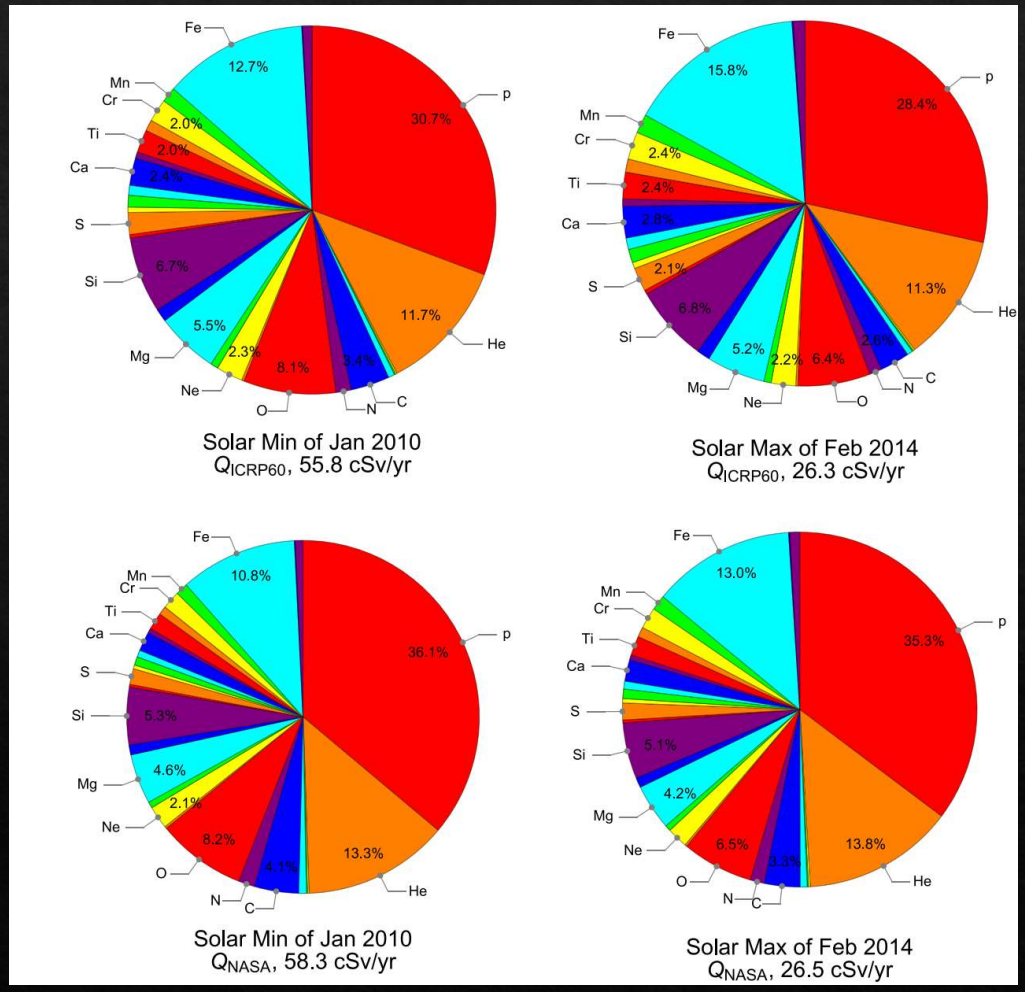

The Sketch Summary of the N.E.S.

Q(R,E) $ICRP_{60}$

Q(R,E) NASA

Tissue weighting factor (WT)

Equivalent Dose rate ($H_{T,R}$) $\sum_T w_T H_{T,R}$ Effective Dose Equivalent rate ($H_{E,R}$) $\sum_R H_{E,R}$ Total Effective Dose Equivalent rate (H_E)

AMS data

Local Interstellar Spectra (LIS)

3D &T.M. (GCR model)

N.E.S.

SPECT(R)
17 /07/ 2006 to 31 /10/ 2019
Bartel Rotation 2360 - 2540

The time series for effective dose equivalent rates and skin dose equivalent rates in the time window (17 July 2006 to 31 October 2019), with genders averaged but two quality factors shown.

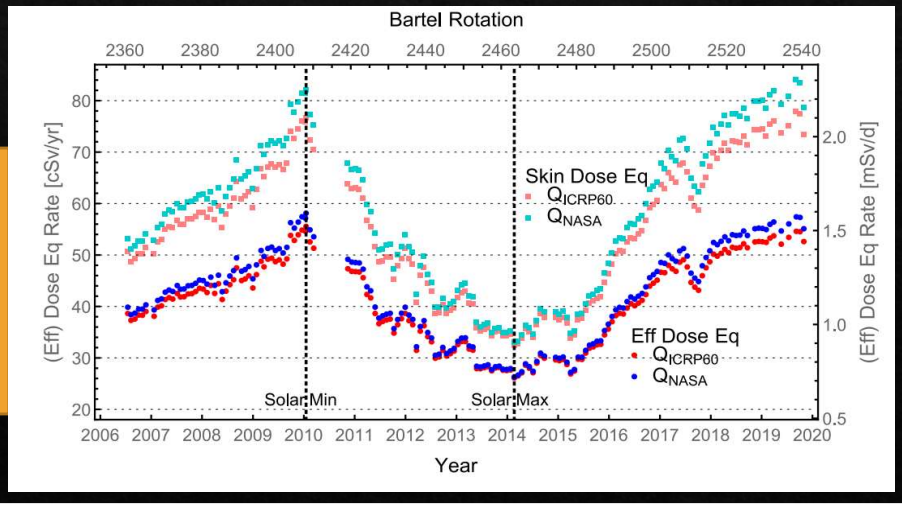

2.3 The Model Precision Checking (1/3)

In Figure 3, it is shown the fractional contributions of all the 28 elements to the unshielded gender-averaged skin dose equivalent.

As seen, the top six contributing elements to the effective dose equivalent also give leading contributions.

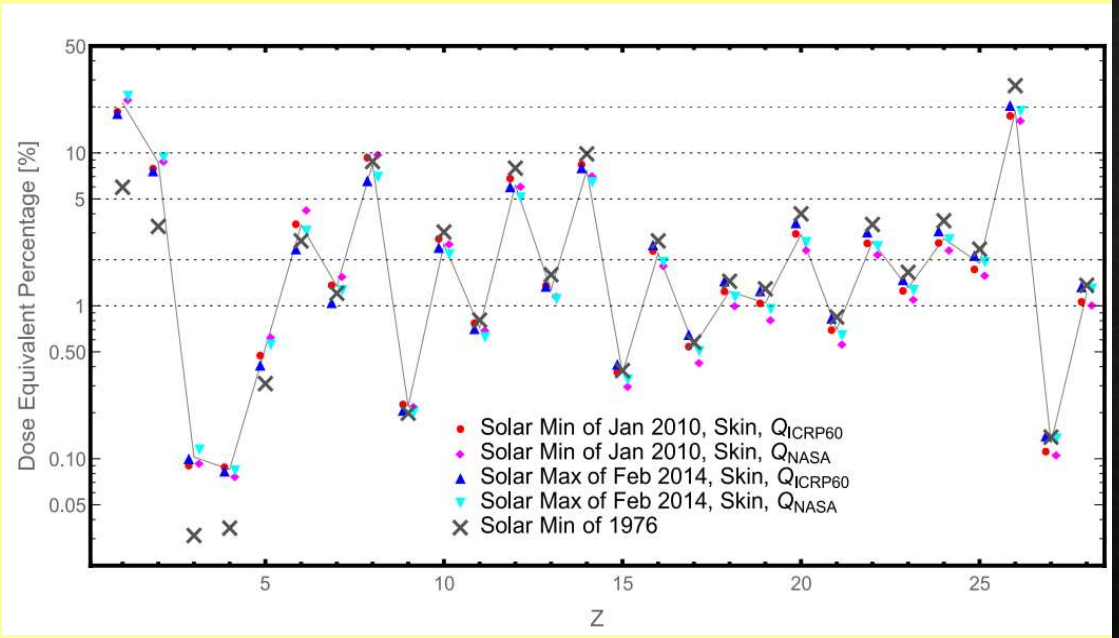

Figure 3. Comparison of the dose equivalent fractional contributions from different elements to the literature results of Durante and Cucinotta (2011), which are based on another solar minimum of the year 1976. Conceptually, the best matching fractions in the calculation are the skin dose equivalent ones at the solar minimum of January 2010 using Q_{ICRP60}, but here shown the combinations of the two quality factors with the solar minimum and maximum (with the solid curves connecting the average of the four fractions to guide the visual). Here the fractions are averaged over genders.

2.3 The Model Precision Checking (2/3)

Here given some detail of the dose rate calculation, which will be used throughout this paper.

Different from the model calculated spectrum, for the AMS-02 measured spectra, each flux value is assigned to a finite rigidity bin interval but not to a single rigidity value.

According to its underlying universal assumption of the $\propto R^{-2.7}$ flux behavior even in a bin, for a bin with rigidity interval R_{min} to R_{max} the single reference rigidity (R_{ref}) is:

$$R_{ref} = \left(\frac{1.7\ (R_{max} - R_{min}}{R_{min}^{-1.7} - R_{max}^{-1.7}}\right)^{\frac{1}{2.7}} \quad (8)$$

2.3 The Model Precision Checking (3/3)

In figure 4, detailed comparisons between the AMS-02 (and PAMELA) measurements and the model calculation have been performed, in the form of time series for the proton and helium channels.

In order to explicitly show the agreement level, in figure, it is plotted the $H_{E,p}(\boldsymbol{R}_M)$ and $H_{E,He}(\boldsymbol{R}_M)$ rates calculated by Equation 7 as interpolated time series, with the AMS-02 directly measured time-dependent spectra, and with our model as well as another model of HelMod for comparison.

It is found that for the GCR model, the absolute relative difference |R*d*| is 0.64% for proton and 0.98% for helium, and for the HelMod model they are 2.9% and 3.8%, respectively

For the HelMod model (M. Boschini et al., 2022) the galactic cosmic ray data is taken from: https://www.helmod.org/index.php/helmod calculators?view=article&id=60:heliospheric modulatorv2018&catid=9:online-resources.

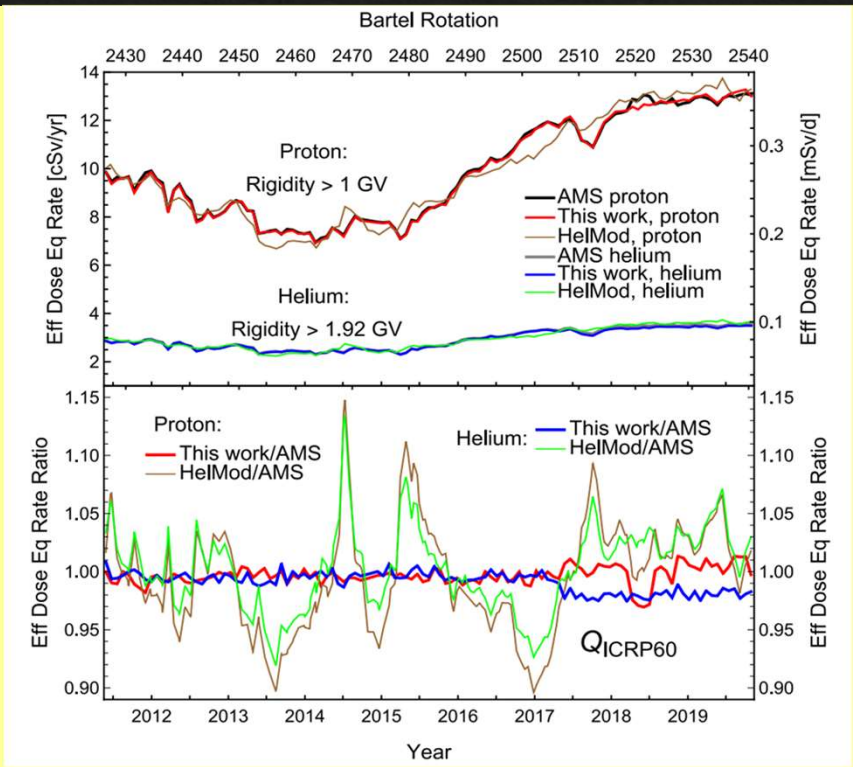

Figure 4. Comparison of the proton and helium channel effective dose equivalent rate contributions using the Q_{ICRP60} definition in the form of interpolated time series, above their specific R_M. For the AMS-02 proton and helium measurements the Bartel rotation averaged spectra before May 2017 were used, after that and till October 2019 the daily spectra in every Bartel rotation were averaged, and if the daily spectrum misses the lowest bin, then it is not counted in the time average

This paper is summarized by the following simple sketch:

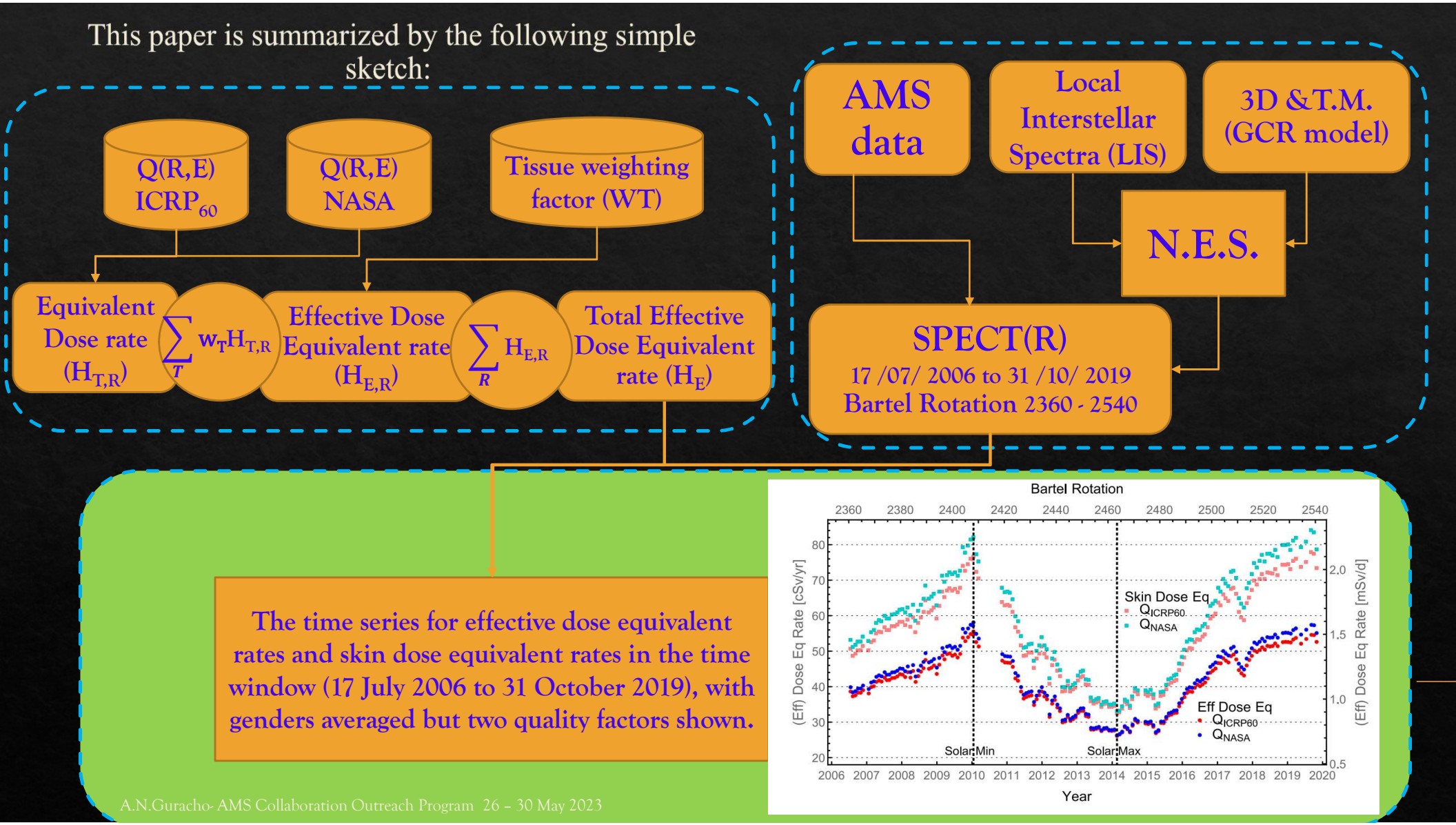

The time series for effective dose equivalent rates and skin dose equivalent rates in the time window (17 July 2006 to 31 October 2019), with genders averaged but two quality factors shown.

3. Results and Discussion
3.1 Comparison Between the Quality Factor Choices

In Figure 5 it is shown both the GCR spectra and the ICRP123 fluence-to-dose conversion coefficients as functions of rigidity, for proton, oxygen, and iron respectively.

Compared with iron, oxygen does have a lower rigidity minimum from measurement, but its fluence-to-dose conversion coefficient peaks (corresponding to the Bragg peak) at an even lower rigidity which is not covered by the rigidity minimum, so its below-minimum fraction is higher.

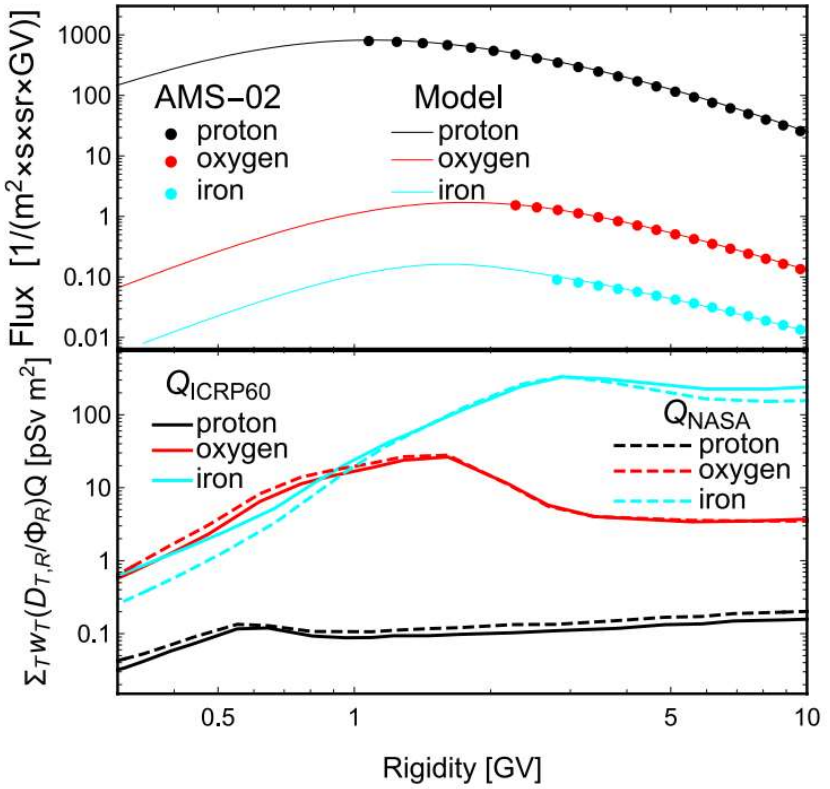

Figure 5. The 7 (8.5) years averaged galactic cosmic ray spectra (upper panel) and the ICRP123 fluence-to-dose conversion coefficient (lower panel), for proton, oxygen and iron respectively.

Table 2
The Effective Dose Equivalent Contribution Calculated at the Solar Minimum, as of January 2010

			p		He		O		Mg		Si		Fe		28 Sum	
	Rate [cSv/yr] at solar minimum	w_T	M	F	M	F	M	F	M	F	M	F	M	F	M	F
Q_{ICRP60}	Red Bone-Marrow	0.12	17.4	17.2	6.5	6.4	4.0	4.2	2.7	2.8	3.3	3.6	6.1	6.4	52.3	53.4
	Colon		17.4	17.6	6.5	6.6	4.0	4.0	2.6	2.7	3.1	3.4	5.8	6.0	51.3	52.2
	Lung		17.2	16.9	6.6	6.6	4.3	4.7	2.9	3.1	3.5	4.3	6.6	7.3	54.3	56.8
	Stomach		17.9	17.2	6.5	6.5	3.6	4.3	2.4	2.8	2.8	3.6	5.3	6.4	49.7	53.3
	Breast		15.8	16.0	6.5	6.5	7.0	6.4	5.1	4.7	6.2	5.2	12.4	11.3	74.5	70.7
	Remainder Tissue		17.4	17.3	6.5	6.5	4.0	4.2	2.7	2.8	3.2	3.6	6.0	6.3	52.1	53.1
	Gonads	0.08	16.8	18.1	6.3	6.2	4.8	3.4	3.7	2.0	4.3	2.7	8.1	4.3	59.3	46.1
	Bladder	0.04	18.0	17.8	6.5	6.6	3.5	3.8	2.1	2.9	2.7	3.4	4.8	6.2	47.7	53.1
	Oesophagus		17.5	17.2	6.6	6.3	3.9	4.3	2.2	2.5	3.0	3.5	5.3	6.2	49.6	52.0
	Liver		17.8	17.5	6.6	6.5	3.8	4.2	2.4	2.7	2.9	3.6	5.4	6.1	50.0	52.8
	Thyroid		16.6	15.8	6.4	6.4	4.7	5.4	3.4	3.6	4.0	4.1	7.8	8.4	57.5	59.7
	Bone Surface	0.01	16.7	16.6	6.5	6.5	5.2	5.3	3.6	3.6	4.3	4.4	8.4	8.4	60.6	60.6
	Brain		16.4	16.3	6.5	6.5	5.5	6.0	3.6	3.8	4.5	5.0	8.8	9.2	62.0	64.1
	Salivary Glands		16.4	15.7	6.4	6.5	5.9	5.8	4.1	4.0	5.2	4.9	10.2	9.5	66.9	64.3
	Skin		14.8	14.6	6.2	6.2	7.3	7.4	5.3	5.4	6.6	6.7	13.7	14.0	**76.7**	**77.4**
	w_T Sum		17.2	17.1	6.5	6.5	4.5	4.6	3.1	3.1	3.7	3.9	7.1	7.1	**55.7**	**55.8**
Q_{NASA}	Red Bone-Marrow	0.12	13.3	13.2	5.1	5.0	1.7	1.7	0.8	0.8	0.9	0.9	1.6	1.6	27.3	27.6
	Colon		22.7	22.0	8.3	8.3	4.5	4.6	2.4	2.5	2.8	2.9	5.5	5.6	58.0	58.0
	Lung		22.5	21.6	8.2	8.2	4.8	5.3	2.7	2.9	3.1	3.4	6.3	6.9	60.8	62.7
	Stomach		22.9	22.5	8.3	8.1	4.1	4.8	2.3	2.6	2.5	3.0	5.0	6.1	56.2	59.7
	Breast		20.2	20.9	8.0	8.0	7.9	7.2	4.8	4.5	5.6	5.2	12.4	11.2	80.4	76.9
	Remainder Tissue		22.4	22.3	8.2	8.2	4.6	4.7	2.5	2.6	2.9	3.0	5.7	6.0	58.5	59.4
	Gonads	0.08	21.8	23.6	7.9	8.2	5.5	3.9	3.5	1.8	3.9	2.2	7.9	3.9	65.6	53.4
	Bladder	0.04	23.2	22.3	8.4	8.3	3.9	4.3	2.0	2.7	2.3	3.1	4.4	5.9	54.4	59.1
	Oesophagus		23.0	23.0	8.3	7.9	4.5	4.9	2.1	2.3	2.7	2.7	5.0	5.8	56.5	58.9
	Liver		23.0	22.5	8.3	8.1	4.2	4.7	2.3	2.6	2.6	2.9	5.1	5.8	56.5	59.0
	Thyroid		22.0	21.7	8.0	8.2	5.4	5.9	3.2	3.3	3.6	3.9	7.5	8.1	64.4	66.8
	Bone Surface	0.01	21.7	21.4	8.0	8.0	5.9	6.0	3.4	3.3	3.9	3.9	8.1	8.1	66.8	66.5
	Brain		21.1	20.7	8.0	8.0	6.3	6.8	3.4	3.6	4.0	4.2	8.5	8.9	67.7	69.5
	Salivary Glands		20.9	20.9	8.0	8.1	6.7	6.5	3.9	3.8	4.7	4.5	10.0	9.3	72.5	70.6
	Skin		19.1	18.8	7.5	7.5	8.2	8.4	5.1	5.2	6.0	6.1	13.7	14.0	**82.1**	**82.8**
	w_T Sum		21.1	21.0	7.8	7.8	4.7	4.8	2.7	2.6	3.1	3.1	6.3	6.2	**58.4**	**58.2**

Note. We expand both genders (Male vs. Female) and the quality factor definitions ($Q_{ICRRP60}$ vs. Q_{NASA}). For each case we show the specific contributions from the top six contributing elements, together with the sum of all the 28 elements. We also show the 15 sensitive organ dose equivalent as defined in the ICRP103 with the corresponding w_T factor themselves, and finally the weighted total effective dose equivalent. Bold values represent that they are more important than the surrounding values and deserve attention in a first glance.

Table 3
The Same as Table 2, but for the Solar Maximum as of February 2014

			p		He		O		Mg		Si		Fe		28 Sum	
	Rate [cSv/yr] at solar maximum	w_T	M	F	M	F	M	F	M	F	M	F	M	F	M	F
Q_{ICRP60}	Red Bone-Marrow	0.12	7.7	7.5	3.1	3.0	1.6	1.6	1.2	1.3	1.6	1.7	3.7	3.9	25.1	25.5
	Colon		7.7	7.7	3.0	3.0	1.5	1.6	1.2	1.2	1.6	1.6	3.6	3.7	24.7	25.1
	Lung		7.5	7.3	3.0	2.9	1.7	1.8	1.3	1.4	1.7	1.9	4.1	4.4	26.1	27.0
	Stomach		7.9	7.6	3.1	3.0	1.5	1.6	1.2	1.3	1.4	1.7	3.4	3.9	24.1	25.5
	Breast		6.6	6.7	2.8	2.8	2.2	2.1	2.0	1.9	2.6	2.4	6.3	6.0	32.3	31.2
	Remainder Tissue		7.7	7.6	3.0	3.0	1.6	1.6	1.2	1.3	1.6	1.7	3.7	3.8	25.1	25.5
	Gonads	0.08	7.5	8.4	2.9	3.0	1.7	1.4	1.6	1.0	2.0	1.3	4.6	2.8	27.5	23.1
	Bladder	0.04	8.1	7.8	3.1	3.1	1.4	1.5	1.0	1.3	1.4	1.7	3.0	3.7	23.5	25.3
	Oesophagus		7.9	7.5	3.1	2.9	1.6	1.7	1.1	1.2	1.5	1.6	3.4	3.8	24.3	25.2
	Liver		7.9	7.6	3.1	3.0	1.5	1.6	1.2	1.3	1.5	1.6	3.4	3.8	24.3	25.3
	Thyroid		7.1	6.7	2.9	2.8	1.7	1.9	1.5	1.6	1.9	2.0	4.5	4.8	26.8	27.6
	Bone Surface	0.01	7.2	7.1	2.9	2.9	1.9	1.9	1.6	1.6	2.0	2.0	4.9	4.9	28.2	28.1
	Brain		6.9	6.8	2.8	2.8	2.0	2.1	1.6	1.7	2.1	2.2	5.2	5.4	29.0	29.7
	Salivary Glands		7.0	6.6	2.7	2.8	2.0	2.0	1.7	1.7	2.3	2.3	5.7	5.4	30.3	29.4
	Skin		6.2	6.1	2.6	2.6	2.2	2.2	2.0	2.0	2.7	2.7	6.9	7.0	**32.8**	**33.0**
	w_T Sum		7.5	7.4	3.0	3.0	1.7	1.7	1.4	1.4	1.8	1.8	4.1	4.2	**26.2**	**26.4**
Q_{NASA}	Red Bone-Marrow	0.12	5.8	5.6	2.4	2.4	0.7	0.7	0.4	0.4	0.4	0.4	0.9	1.0	12.6	12.6
	Colon		10.2	9.9	4.0	4.0	1.7	1.7	1.1	1.1	1.3	1.3	3.2	3.3	27.1	27.0
	Lung		10.0	9.5	3.9	3.8	1.8	1.9	1.2	1.2	1.4	1.6	3.6	4.0	28.1	28.6
	Stomach		10.4	10.0	4.0	3.8	1.6	1.8	1.0	1.1	1.2	1.4	3.0	3.5	26.5	27.6
	Breast		8.7	8.9	3.5	3.5	2.3	2.2	1.7	1.6	2.1	2.0	5.9	5.6	33.2	32.3
	Remainder Tissue		10.1	9.9	4.0	3.9	1.7	1.8	1.1	1.1	1.3	1.4	3.3	3.4	27.3	27.5
	Gonads	0.08	9.7	10.8	3.7	4.0	1.9	1.6	1.4	0.9	1.6	1.1	4.1	2.4	29.2	25.8
	Bladder	0.04	10.6	10.1	4.1	4.0	1.6	1.6	0.9	1.1	1.1	1.4	2.7	3.3	26.1	27.3
	Oesophagus		10.4	10.3	4.0	3.8	1.8	1.9	1.0	1.0	1.3	1.3	3.0	3.4	26.7	27.6
	Liver		10.3	10.0	4.0	3.9	1.7	1.8	1.0	1.1	1.2	1.4	3.0	3.4	26.6	27.4
	Thyroid		9.7	9.5	3.7	3.7	1.9	2.1	1.3	1.3	1.6	1.6	4.1	4.4	28.9	29.7
	Bone Surface	0.01	9.5	9.3	3.7	3.6	2.0	2.1	1.4	1.4	1.7	1.7	4.4	4.4	29.8	29.7
	Brain		9.1	8.9	3.6	3.5	2.2	2.3	1.4	1.5	1.7	1.8	4.7	4.9	30.3	30.7
	Salivary Glands		9.0	9.0	3.5	3.6	2.2	2.2	1.5	1.5	1.9	1.9	5.2	4.9	31.3	30.8
	Skin		8.2	8.0	3.2	3.2	2.4	2.4	1.7	1.8	2.2	2.2	6.4	6.5	**33.4**	**33.5**
	w_T Sum		9.4	9.3	3.7	3.6	1.7	1.7	1.1	1.1	1.3	1.4	3.4	3.5	**26.5**	**26.5**

Note. Bold values represent that they are more important than the surrounding values and deserve attention in a first glance.

3.2 Comparison Between the Effective Dose Equivalent and Dose Equivalent (1/2)

In Figure 6 it is shown the results for both the effective dose equivalent rate which is the w_T weighted sum of the dose equivalent rates for all 15 sensitive tissues/organs, and the skin dose equivalent rate as one instance.

The former has better medical meaning according to ICRP103, while the latter is conceptually more appropriate to be compared to most previous calculations and measurements.

According to the approximation which is widely made in most previous dose equivalent calculations or measurements in literature, the absorbed dose (mainly due to the absorption of the low energy secondary particles) is given by the energy loss of the high energy primary particle as:

$$D = \frac{dE}{dm} = N\left(\frac{dE}{dx}\right)\left(\frac{dx}{dm}\right) = \frac{N}{A}\left(\frac{dE}{dx}\right)\frac{1}{\frac{dm}{A\,dx}} = \Phi\, LET\, \frac{1}{\rho} \quad \ldots \quad (9)$$

then the quality factor Q is multiplied to obtain the dose equivalent.

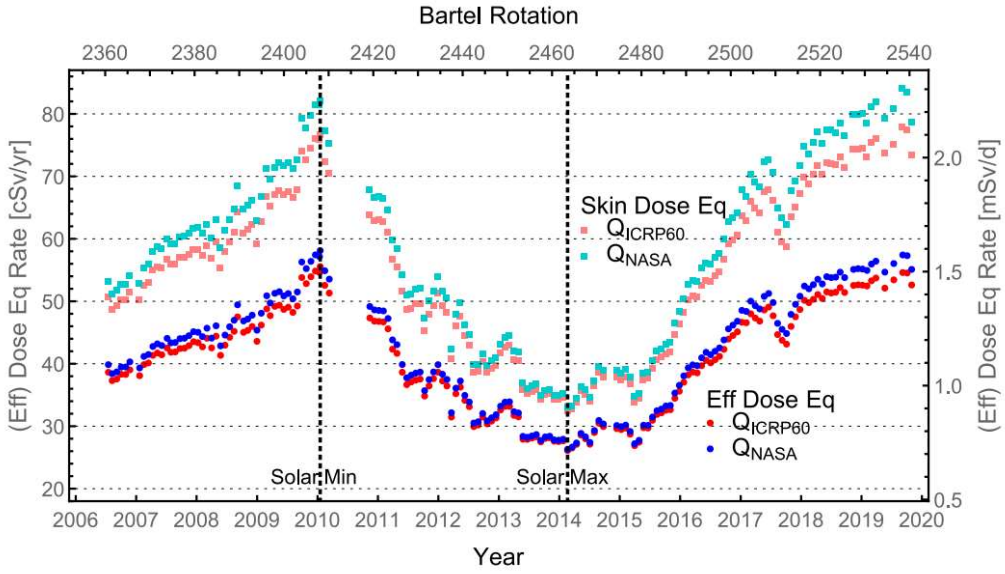

Figure 6. The time series for effective dose equivalent rates and skin dose equivalent rates in the time window (17 July 2006 to 31 October 2019), with genders averaged but two quality factors shown. Rate calculations are usually for each Bartel period but are not always available such as in the year 2010.

3.2 Comparison Between the Effective Dose Equivalent and Dose Equivalent

The skin dose equivalent (or the literature dose equivalent) being larger than the effective dose equivalent is a natural consequence of the self-shielding effect, that, unlike the skin, most medically important organs/tissue (with large w_{Ts}) are buried deep in the human body, so the radiation flux there has been significantly reduced or changed.

Another observation from the comparison between the effective dose equivalent and the skin dose equivalent is the difference in the fractional contribution.

Comparing Figures 2 and 3, from the effective dose equivalent to the skin dose equivalent, the proton fractional contribution reduces from about 30% to about 20%, and the iron fractional contribution increases from about 13% to about 19%. This can also be attributed to the self-shielding effects. Because the nucleus' LET is proportional to Z^2 but the kinetic energy is generally proportional to its nucleon number A, for heavy ions the former wins and they tend to be stopped at a shallower position, enhancing the surface energy deposit.

3.3 Comparison With Literature Results (1/2)

In Figure 4, the GCR model traces much more closely, the time variation of the GCR flux than the HelMod model and gives a better time-dependent dose rate. This is because the GCR model does diffusion and drift coefficients fitting for every Bartal rotation, as a tradeoff for the forecast capability.

For the fractional contribution from different elements, at the effective dose equivalent level, the results (see Figure 2) are quite similar to Naito et al. (2020) which also uses ICRP123.

At the dose equivalent level, the results of this paper are compared to Durante and Cucinotta (2011) in Figure 3. Only in the combination of solar maximum with the Q_{ICRP60} definition, iron gives a slightly larger fractional contribution than proton, which is consistent with the literature result of Durante and Cucinotta (2011).

By modeling the GCR propagation in the magnetosphere and its interaction with the top part of the atmosphere, in the future, it can be able to reproduce the GCR spectra and the radiation dose on such orbit.

3.3 Comparison With Literature Results (2/2)

In conclusion, the recent GCR model with the AMS-02 data has significantly reduced the radiation dose uncertainty from the GCR spectra. At $\lesssim$2%, its uncertainty is subdominant to other uncertainty sources in the computation of radiation dose.

The new (effective) dose equivalent rates as a time series from 2006 to 2019 and the rate details at the solar minimum (January 2010) and maximum (February 2014) are provided for direct practical use.

Thank You